Effect of Loss on Multiplexed Single-Photon Sources

Damien Bonneau*,[1] Gabriel J. Mendoza*,[1] Jeremy L. O'Brien,[1] and Mark G. Thompson†[1]

[1] *Centre for Quantum Photonics, H. H. Wills Physics Laboratory & Department of Electrical and Electronic Engineering, University of Bristol, Merchant Venturers Building, Woodland Road, Bristol, BS8 1UB, UK*

An on-demand single-photon source is a key requirement for scaling many optical quantum technologies. A promising approach to realize an on-demand single-photon source is to multiplex an array of heralded single-photon sources using an active optical switching network. However, the performance of multiplexed sources is degraded by photon loss in the optical components and the non-unit detection efficiency of the heralding detectors. We provide a theoretical description of a general multiplexed single-photon source with lossy components and derive expressions for the output probabilities of single-photon emission and multi-photon contamination. We apply these expressions to three specific multiplexing source architectures and consider their tradeoffs in design and performance. To assess the effect of lossy components on near- and long-term experimental goals, we simulate the multiplexed sources when used for many-photon state generation under various amounts of component loss. We find that with a multiplexed source composed of switches with $\sim 0.2-0.4$ dB loss and high efficiency number-resolving detectors, a single-photon source capable of efficiently producing 20-40 photon states with low multi-photon contamination is possible, offering the possibility of unlocking new classes of experiments and technologies.

arXiv:1409.5341v2 [quant-ph] 29 Apr 2015

Introduction

An on-demand single-photon source is a key requirement for many optical quantum technologies, including quantum key distribution schemes using quantum repeaters [1], quantum metrology using photon-number states [2][3], analog quantum simulators [4], and the boson sampling machine [5]. The ultimate optical quantum technology may be the quantum computer [6], capable of efficient integer factorization and digital quantum simulation [7][8], which relies critically on the development of a high-performance, on-demand photon source in order to efficiently generate large quantum resource states [9][10].

While research efforts continue in developing on-demand single-photon sources using atomic systems, achieving high spectral purity and high collection efficiency simultaneously remains a challenge [11]. An alternative approach commonly used in quantum optics experiments is heralded single-photon sources (HSPSs) such as those based on spontaneous parametric down-conversion (SPDC) or spontaneous four-wave mixing (SFWM): parametric processes which use a pump laser in a nonlinear material to spontaneously generate photon pairs (Fig. 1a). Detecting one of the photons using a single-photon detector will herald the presence of the paired photon to be input into the quantum circuit. Parametric sources are capable of producing single photons with high spectral purity [11], benefit from a well-defined wave vector leading to high collection efficiency [12], and have no mode-mismatch when integrated on the same monolithic substrate as the subsequent circuit. However, parametric sources are inherently inefficient, due to the thermal nature of the output statistics and the requirement to keep the multi-photon emissions low, resulting in a maximum single-photon output probability of 25% [13]. For applications requiring many single photons, the probability of successfully generating N single photons simultaneously with N HSPSs decreases as N becomes large, severely limiting the size of practical circuits.

An approach to overcome all of the scaling problems with HSPSs is the *multiplexed* (MUX) single-photon source [14], which uses an array of HSPSs, delay lines, electronics for classical logic operations, and an active optical switching network to approximate a true on-demand source (Fig. 1b). Using an array of HSPSs as a collective unit means that the probability that at least one of the HSPSs emits a single photon is high, while a switching network driven by the heralding signals is used to route the generated photon into a specific spatial-temporal output mode. This results in the near-deterministic generation of single photons, allowing for much larger quantum circuits than could be feasibly built with HSPSs without active multiplexing. MUX sources inherit the same benefits as parametric HSPSs, including their mature theoretical and experimental investigation, and are especially appealing due the prospects of a fully integrated device with existing fabrication processes.

Several theoretical schemes have been previously investigated [15–23] and experimental work using bulk [24] and

* Authors DB and GJM contributed equally to this work.
† mark.thompson@bristol.ac.uk

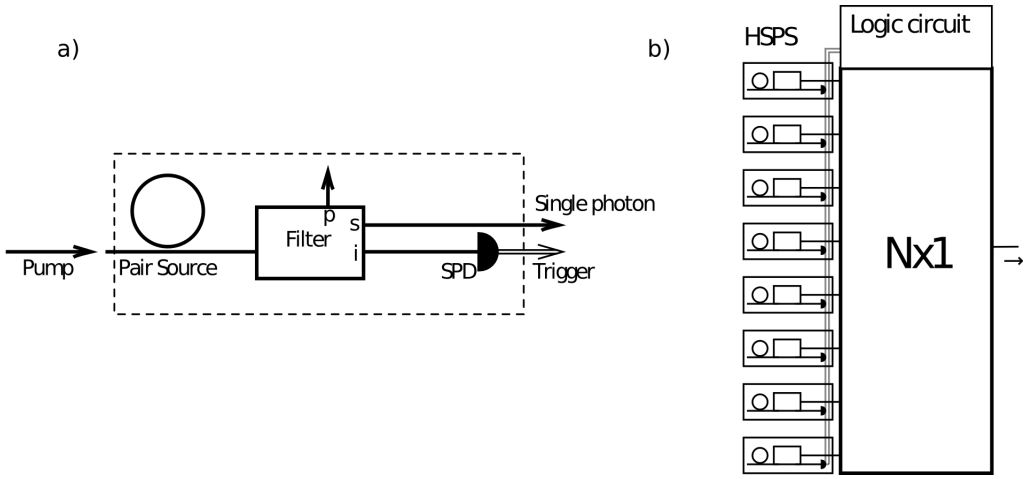

Figure 1: a) Heralded single-photon source (HSPS). A laser pumps a parametric pair source which spontaneously emits a signal and an idler photon. A filter separates the pump, signal, and idler. The idler photon is detected using a single-photon detector (SPD), heralding the presence of the signal photon. b) A general multiplexed (MUX) single-photon source. N HSPSs are pumped simultaneously; the idler photons are detected while the signal photons are stored in a long delay line. A classical logic unit determines the configuration for the $N \times 1$ switching network based on the detection signals, routing a successfully generated single photon to the output.

integrated [25][26] components has been demonstrated. Previous work has highlighted the fundamental constraints for creating pure states using parametric processes assuming ideal MUX components [13]. However, in real physical settings, non-ideal components will limit the efficiency and output fidelity of MUX sources. The most significant sources of error in multiplexed sources are likely to be photon loss in the optical components and the non-unit detection efficiency of the heralding detectors (which can also be viewed as photon loss). Assessing the suitability of a MUX sources using lossy components is an important consideration for many quantum photonic technologies, in particular the large-scale quantum computer, as fault-tolerance thresholds will place demands on the required source efficiency and fidelity [10][27].

The aim of this work is to assess the impact of photon loss on the performance of multiplexed single-photon sources. We start by detailing the HSPS, which is a key building block of all the MUX sources, and include the effect of photon loss and non-unit efficiency number-resolving and non-number resolving detectors. We extend this description to general multiplexed single-photon sources with lossy components and derive expressions for single-photon and multi-photon emission probabilities. We then apply these expressions to three specific multiplexing source architectures and consider their tradeoffs in design and performance. To assess the effect of lossy components on near- and long-term experimental goals, we simulate the multiplexed sources when used for many-photon state generation under various amounts of component loss. We conclude by discussing the prospects of using the different MUX architectures with realistic components for near- and long-term experimental goals.

I. THE HERALDED SINGLE PHOTON SOURCE

A. Theory and figures of merit

All the MUX sources we consider are composed of a core component called the heralded single photon source (HSPS) (Fig. 1a). A HSPS is a non-deterministic source with a logic output set to 1 when it emits a photon and set to 0 otherwise. We consider a HSPS composed of 1) a photon pair generation stage in which photons are produced at non-degenerate wavelengths λ_s (signal) and λ_i (idler), 2) a filter which removes the pump and separates the signal from the idler into two different paths, and 3) a detector on the idler arm which heralds the emission of the signal photon. For now, we assume the photon pairs are generated as a biphoton two-mode squeezed vacuum state such that their joint spectrum is disentangled [28]. Furthermore, we assume that all signal photons produced from different HSPSs are perfectly indistinguishable in all degrees of freedom except for the spatial mode in which they are generated.

The source is characterised by a squeezing parameter ξ, determined by the pump intensity and strength of the nonlinearity, a trigger probability p_{trig}, the probability for the heralded state to be a single photon p_{single}, also called

the state fidelity or heralding efficiency, and the probability for the heralded state to be contaminated with multiple photons, p_{multi}. Quantifying multi-photon contamination separately from vacuum emissions is especially important; vacuum emissions can be treated as effective loss in a linear optical quantum circuit while multi-photon events can result in other types of errors, and linear optical quantum circuits have been shown to have a much higher tolerance to loss than to other errors [10].

We aim at deriving expressions for p_{trig}, p_{single} , and p_{multi} for the case in which the heralding detector is number-resolving and the case in which the detector is non-number resolving (also called a threshold detector). The state produced by the pair source, assuming spectral disentanglement, is of the form [29]:

$$|\psi\rangle = \sqrt{1-|\xi|^2}\left(|0\rangle_i|0\rangle_s + \xi|1\rangle_i|1\rangle_s + \sum_{n=2}^{\infty}\xi^n|n\rangle_i|n\rangle_s\right), \tag{1}$$

where i and s are the idler and signal modes. In practice, sources and filters have losses, and the heralding detector does not have a unit efficiency detection. We call η_i the global collection efficiency on the idler arm accounting for all these effects, and η_s is the overall transmission on the signal arm accounting for losses in the sources and filters. Each lossy component is modelled as an ideal component preceded by an ideal beamsplitter with a non-unit transmission probability. The full state, after accounting for losses and tracing over loss modes, can therefore be written:

$$\hat{\rho} = \left(1-|\xi|^2\right)\left(\sum_{n=0}^{\infty}|\xi|^{2n}\sum_{p=0}^{n}\sum_{k=0}^{n}C_n^p\eta_i^p\left(1-\eta_i\right)^{n-p}C_n^k\eta_s^k\left(1-\eta_s\right)^{n-k}\hat{\rho}_{p,k}\right), \tag{2}$$

where $\hat{\rho}_{p,k} = |p\rangle_i|k\rangle_s\langle p|_i\langle k|_s$ and C_n^k is the binomial coefficient.

This expression will be the starting point to derive $p_{trig\,D}$, $p_{single\,D}$, and $p_{multi\,D}$ for the two detection schemes. In this paper we use the subscript D on expressions to indicate the type of detector considered: NRD for number-resolving detector and TD for threshold detector. Detailed derivations can be found in Appendix A.

B. Heralded single-photon source parameters

Threshold Detector

Starting with the reduced state (Eq. 2) and tracing out the signal mode, the probability for the detector on the idler arm to trigger is given by summing all the contribution of the states having at least one photon and is given by:

$$p_{trig\,TD} = \frac{|\xi|^2\eta_i}{1-|\xi|^2\left(1-\eta_i\right)}. \tag{3}$$

The heralded state in the signal arm is expressed, renormalizing by dividing by $p_{trig\,TD}$, as:

$$\hat{\rho}_{heralded\,TD} = \frac{\left(1-|\xi|^2\right)}{p_{trig\,TD}}\left(\sum_{n=1}^{\infty}|\xi|^{2n}\sum_{p=1}^{n}\sum_{k=0}^{n}C_n^p\eta_i^p\left(1-\eta_i\right)^{n-p}C_n^k\eta_s^k\left(1-\eta_s\right)^{n-k}|k\rangle_s\langle k|_s\right). \tag{4}$$

We can compute the probability that the heralded state is a single-photon using $p_{single\,TD} = \langle 1|_s\hat{\rho}_{heralded\,TD}|1\rangle_s$:

$$p_{single\,TD} = \left(1-|\xi|^2\right)\eta_s\frac{\left[1-\left(|\xi|^2\left(1-\eta_s\right)\right)^2\left(1-\eta_i\right)\right]\left[1-|\xi|^2\left(1-\eta_i\right)\right]}{\left[1-|\xi|^2\left(1-\eta_s\right)\right]^2\left[1-|\xi|^2\left(1-\eta_s\right)\left(1-\eta_i\right)\right]^2}. \tag{5}$$

The probability that the heralded state contains multi-photon contamination is given by $p_{multi\,TD} = \sum_{m=2}^{\infty}\langle m|_s\hat{\rho}_{heralded\,TD}|m\rangle_s$:

$$p_{multi\,TD} = \frac{Z_{TD}}{p_{trig\,TD}} - p_{single\,TD}, \tag{6}$$

with

$$Z_{TD} = \left(1 - |\xi|^2\right)|\xi|^2 \left(\frac{1}{1-|\xi|^2} + \frac{(1-\eta_s)(1-\eta_i)}{1-|\xi|^2(1-\eta_s)(1-\eta_i)} - \frac{(1-\eta_i)}{1-|\xi|^2(1-\eta_i)} - \frac{(1-\eta_s)}{1-|\xi|^2(1-\eta_s)}\right). \tag{7}$$

Note that we can also similarly derive an expression for the probability that the heralded state is any Fock number state using $\langle n|_s \hat{\rho}_{heralded\,TD} |n\rangle_s$.

Number-resolving detector

We now consider the case in which the detector is number resolving. In practice, we only need to discriminate the single-photon state from the vacuum and from states having two or more photons. Therefore, the detector does not need to be able to distinguish between two and $N > 2$ photon states. Starting again from Eq. 2, tracing out the signal mode and calculating the probability to get only one photon gives:

$$p_{trig\,NRD} = \frac{\left(1 - |\xi|^2\right)|\xi|^2 \eta_i}{\left(1 - (1-\eta_i)|\xi|^2\right)^2}. \tag{8}$$

The corresponding heralded state is:

$$\hat{\rho}_{heralded\,NRD} = \frac{\left(1-|\xi|^2\right)}{p_{trig\,NRD}}\eta_i \left(\sum_{n=1}^{\infty} |\xi|^{2n} n (1-\eta_i)^{n-1} \sum_{k=0}^{n} C_n^k \eta_s^k (1-\eta_s)^{n-k} |k\rangle_s \langle k|_s\right). \tag{9}$$

As in the previous case, we can compute the probability the heralded state contains one photon $p_{single\,NRD} = \langle 1|_s \hat{\rho}_{heralded\,NRD} |1\rangle_s$:

$$p_{single\,NRD} = \left(1 - (1-\eta_i)|\xi|^2\right)^2 \eta_s \left(\frac{\left(1 + (1-\eta_i)(1-\eta_s)|\xi|^2\right)}{\left(1-(1-\eta_i)(1-\eta_s)|\xi|^2\right)^3}\right). \tag{10}$$

Not surprisingly, contrary to the previous case, number-resolving detectors enable unit fidelity in the absence of losses ($p_{single\,NRD} = 1$ when $\eta_i = \eta_s = 1$). The probability for the heralded state to contain multi-photon contamination is given by:

$$p_{multi\,NRD} = \eta_s \frac{1 - (1-\eta_s)\left(|\xi|^2(1-\eta_i)\right)^2}{\left(1 - |\xi|^2(1-\eta_i)(1-\eta_s)\right)^2} - p_{single\,NRD}. \tag{11}$$

We can again similarly derive an expression for the probability that the heralded state is any Fock number state using $\langle n|_s \hat{\rho}_{heralded\,NRD} |n\rangle_s$.

C. Discussion

We now have a complete framework for characterizing any HSPS. We assumed no joint spectral entanglement between photons in a generated photon pair. However, we can account for joint spectral entanglement by redefining

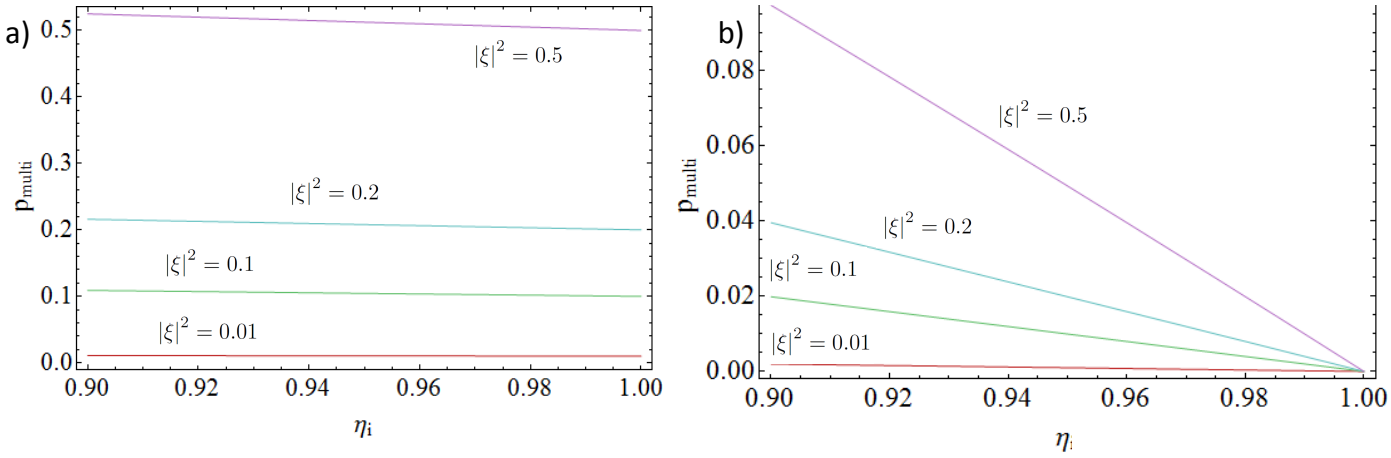

Figure 2: Probability of multi-photon emission p_{multi} from a HSPS as a function of the efficiency in the idler arm η_i for different squeezing parameters $|\xi|^2$ using (a) a threshold detector, (b) a number-resolving detector.

the fidelity as $p'_{single\,D} = p_{single\,D} \times P$ where P is the purity of the heralded single photon. Recall that, in the ideal case of lossless components, the probability $p_{trig\,NRD}$ of heralding a unit fidelity single photon is bounded by 0.25 (achieved when $|\xi|^2 = 0.5$ maximizes the probability $|\xi|^2\left(1-|\xi|^2\right)$). Clearly, HSPS do not suffice on their own to function as a near-deterministic single-photon source, providing in the ideal scenario one photon every four pulses on average.

As we will see in Sec. II, the probability of multi-photon contamination from individual HSPSs approximates the probability of multi-photon contamination from MUX sources. We therefore graph $p_{multi\,D}$ as a function of idler transmission η_i for several squeezing parameters $|\xi|^2$ in Figs. 2a and 2b. To focus on the effect of η_i, we take $\eta_s = 1$; the plots therefore serve as an upper bound on $p_{multi\,D}$. We see that threshold detectors only reliably herald a single-photon state for very low levels of squeezing, while number-resolving detectors achieve a much lower level of contamination with the same squeezing parameter. With number-resolving detectors, 10% loss in the idler arm ($n_i = 0.90$), and pumping with $p_{pair} = 0.09$ ($|\xi|^2 = 0.1$), the multi-photon contamination level is almost an order of magnitude lower (~ 0.02) compared with that of threshold detectors with the same squeezing parameter (~ 0.1). Despite their enhanced performance compared to threshold detectors, number-resolving detectors with the highest pumping parameters are not immune to loss; even 10% loss in the idler arm with $p_{pair} = 0.25$ ($|\xi|^2 = 0.5$) results in a probability of multi-photon contamination of ~ 0.1. Achieving a lower level of contamination requires a reduction in either the squeezing parameter or the loss in the idler arm.

In Sec. II we will show that a practical multiplexed source will require operation in the strong pumping regime, thus showing that threshold detectors can not be used for multiplexed sources with the highest efficiency and low levels of multi-photon contamination. For this reason, and due to space constraints, we will only consider number-resolving detectors in the remainder of the paper. However, the derived expression for threshold detectors can still be used in the framework for multiplexed sources.

II. MULTIPLEXED SINGLE-PHOTON SOURCES

A. General considerations

A general MUX source can be characterised in a similar way to the HSPS. The probability per clock-cycle that at least one HSPS in an array of N HSPSs triggers is given by:

$$p_{trig}^{MUX} = 1 - (1 - p_{trig})^N, \tag{12}$$

and the probability per clock-cycle that at least one source emits a triggered single-photon is:

$$p_1 = p_{single}\left(1 - (1 - p_{trig})^N\right). \tag{13}$$

p_1 can in principle be made arbitrarily close to one, such that a near-deterministic single-photon source (>99% emission probability) can be made out of 17 HSPSs using a lossless switching network to route the photon from the HSPS which triggered to the output [13]. However, in any implementation, the switching network will have loss due to the optical delay lines—required for allowing enough time to reconfigure the switching network upon trigger from the HSPS—and the intrinsic loss of the switch components, for example 2×2 couplers and phase modulators for MZI-type switches (we will assume all 2×2 switches are MZI-type switches). The network loss, $\eta_{network}(N)$, is proportional to the number of sources used in the MUX source, since additional sources require a larger switching network for routing. Provided the losses are equally distributed in the network (this assumption holds for two of the three schemes presented in the further sections), the network loss applies the same amount of loss to every HSPS.

For switching networks with balanced loss, the probability per clock-cycle for a MUX source to emit a single photon, conditioned on the MUX source triggering, is given by p_{single}^{MUX}, and is calculated from Eq. 5 or 10 (depending on the type of detector) by replacing η_s in the expression with the full transmission $\eta_s\eta_{network}(N)$. Similarly, the probability for a MUX source to emit multi-photon contamination, conditioned on the MUX source triggering, is given by p_{multi}^{MUX}, and is calculated from either Eq. 6 or 11 (depending on the type of detector) by replacing η_s in the expression with the full transmission $\eta_s\eta_{network}(N)$. Using this definition of p_{single}^{MUX}, it then follows that the probability per clock-cycle for a multiplexed source to emit a triggered single-photon can be written:

$$q_{MUX} = p_{single}^{MUX} \times p_{trig}^{MUX}. \tag{14}$$

For switching networks with balanced loss, a convenient lower bound for this probability is given by:

$$q_{MUX}^{*} = p_{single} \times p_{trig}^{MUX} \times \eta_{network}(N), \tag{15}$$

which uses only the single-photon emission probability from the HSPSs and neglects cases in which multi-photon contamination from the HSPS reduces to a single-photon due to loss from the switching network.

For a multiplexed source pumped by a pulsed laser with repetition rate R, the emission rate of triggered single-photons is:

$$R_{MUX} = R \times q_{MUX}.$$

Large-scale linear optical experiments require M multiplexed sources in parallel for generating M single photons. The M-photon state is heralded by the simultaneous triggering of all M MUX sources (at least one HSPS per MUX source). For a source pumped by a pulse laser with repetition rate R, the M-photon generation rate is:

$$R_{MUX}^{M} = R \times \left(q_{MUX}\right)^{M}. \tag{16}$$

The multi-photon contamination probability conditioned on heralding the M-photon state is:

$$p_{multi}^{MUX\,M} = 1 - \left(1 - p_{multi}^{MUX}\right)^{M}. \tag{17}$$

The analysis so far has been kept general, and can be applied to any MUX source with balanced network loss. In the next sections we focus on three specific architectures.

While photon loss and inefficient detectors are likely to be the dominant source of error for the near-term implementation of MUX sources, we note that there are other sources of error which will also have an effect on MUX performance. These include dark counts from single-photon detectors [30], mode-mismatch [31], and circuit faults. These effects are left to a future analysis. We also assume that the detector deadtimes are smaller than the system clock period, and therefore loss effects due to detector deadtimes are not considered in our current work.

B. Log-tree source

The first MUX implementation we consider is called the log-tree source. In this scheme, the output optical ports of N HSPS sources are connected to an $N\times1$ reconfigurable switch, which is a logarithmic tree composed of 2×2

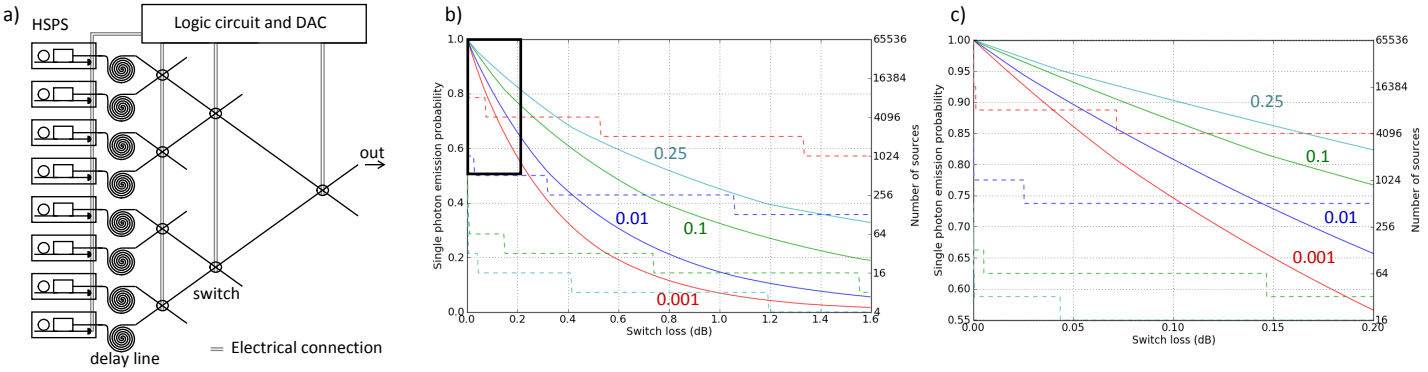

Figure 3: (a) Log-tree MUX source. The trigger output of each HSPS is linked to logic circuit which configures the setting of each switch in the network. (b,c) Maximal probability of triggered single-photon emission and optimal number of HSPSs per MUX source as a function of the switch loss. Each color represents a given probability to trigger p_{trig}. The plain lines (left axis) represent the maximal single-photon emission probability for a given switch loss. The dashed line (right axis) is the number of HSPSs needed to attain the maximal single-photon emission probability for a given switch loss. (c) Shows detail at low switch losses (<0.2 dB). We plot the graphs with $\eta_{delay} = 1$ and $p_{single} = 1$.

switches (Fig. 3a). Using N sources requires a log tree with a depth of $\lceil \frac{\ln N}{\ln 2} \rceil$ 2×2 switches in order to route any of the N sources to the output. The signal photons are stored in delay lines as the electrical trigger output is sent to a logic circuit and the network configuration is determined and set.

The network loss is given by $\eta_{network}(N) = \eta^{\lceil \frac{\ln N}{\ln 2} \rceil} \eta_{delay}$ where η is the transmission of a switch in the log tree network and η_{delay} is the loss of the delay line. From Eq. 14, the probability per clock-cycle for the log-tree multiplexed source to emit a triggered single-photon is given by:

$$q_{tree} = p_{single}^{tree} \left(1 - (1 - p_{trig})^N\right). \tag{18}$$

and has the lower bound (Eq. 15):

$$q_{tree}^* = p_{single} \left(1 - (1 - p_{trig})^N\right) \eta^{\lceil \frac{\ln N}{\ln 2} \rceil} \eta_{delay}. \tag{19}$$

The optimal number of sources for a given switch loss is found by numerically finding the N which maximizes Eq. (19). To study the effect of switching loss in isolation from other sources of loss, the optimal N and q_{tree}^* with $\eta_{delay} = 1$ and $p_{single} = 1$ are plotted as a function of the 2×2 switch loss in Fig. 3b and 3c. As expected, we see that the probability of triggered single-photon emission tends towards 1 in the limit of low switching loss for all trigger probabilities. The number of HSPSs required in the weak pump regime ($p_{trig} < 0.01$) is likely to be impractical: obtaining a probability of single photon emission $q_{tree}^* > 0.9$ with $p_{trig} = 0.01$ requires 512 sources in parallel and switches with 0.05 dB loss (~ 0.989 transmission). Obtaining $q_{tree}^* > 0.9$ with $p_{trig} = 0.1$ requires 64 sources in parallel and switches with 0.07 dB loss (~ 0.984 transmission). With the maximum trigger probability $p_{trig} = 0.25$, only 16 sources and switches with 0.1 dB loss (~ 0.977 transmission) are required.

Because the switching network is balanced, the probability for a triggered log-tree MUX source to emit multi-photon contamination p_{multi}^{MUX} is calculated as explained in Sec. II A using $\eta_{network}(N) = \eta^{\lceil \frac{\ln N}{\ln 2} \rceil} \eta_{delay}$. Since the loss from the switching network can only decrease p_{multi}^{MUX}, the multi-photon contamination probabilities for the HSPSs in Figs. 2a) and b) serve as valid upper bounds for p_{multi}^{MUX}. We will consider these expressions further when we consider M-photon state generation in Sec. III.

C. Generalized Mach-Zehnder interferometer

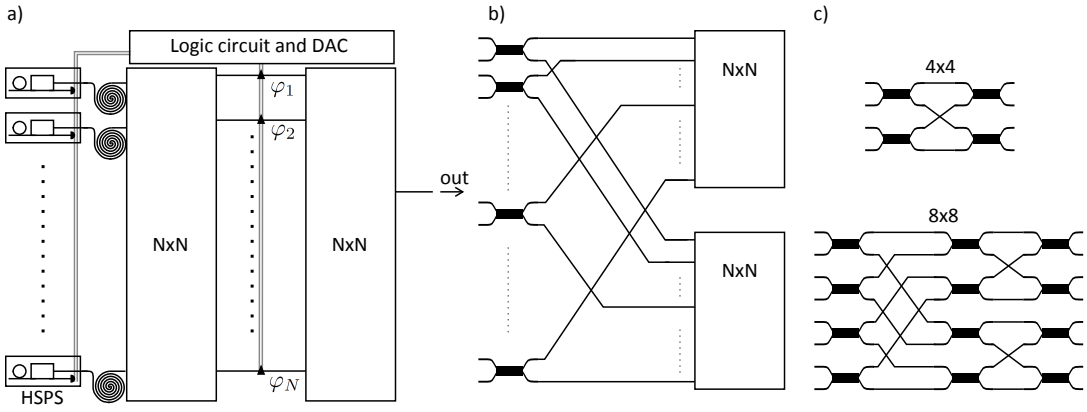

Figure 4: Generalized Mach-Zehnder MUX source. a) Multiplexing N HSPSs using a generalized MZI composed of two $N \times N$ balanced splitters enclosing N arms each having a tuneable phase φ_i. b) Recursive definition of the $N \times N$ balanced coupler. A $2N \times 2N$ balanced coupler is composed of N 2×2 couplers each having one arm connected to a $N \times N$ balanced coupler and the other arm connected to another $N \times N$ balanced coupler. c) Examples of circuit layouts for the 4×4 and 8×8 balanced couplers.

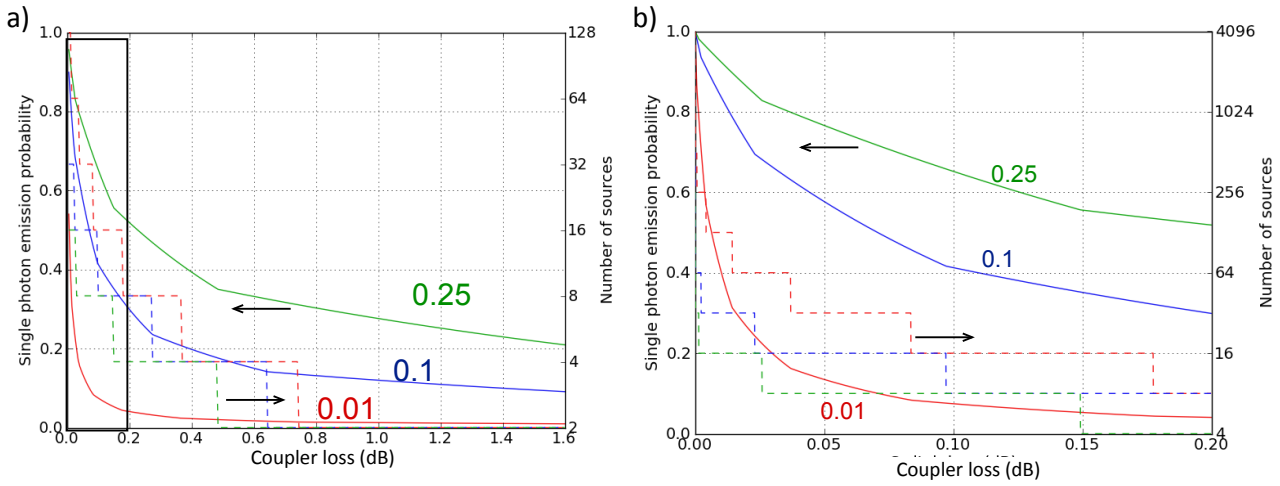

Figure 5: GMZ MUX source: Maximal probability of triggered single-photon emission and optimal number of HSPSs per MUX source as a function of the switch loss. Each color represents a given probability to trigger p_{trig}. The plain lines (left axis) represent the maximal single-photon emission probability for a given coupler loss. The dashed line (right axis) is the number of HSPSs needed to attain the maximal single-photon emission probability for a given coupler loss. (c) Shows detail at low coupler losses (<0.2 dB). We plot the graphs with η_{delay},$\eta_{modulator}$, and $p_{single} = 1$.

Like the log-tree source, this scheme also uses N HSPS sources connected to a $N \times 1$ reconfigurable switch (Fig. 4a). However, here the $N \times 1$ switch is a generalized Mach-Zehnder interferometer (GMZ) - composed of two $N \times N$ balanced splitters enclosing N phase modulators. N phase modulators are sufficient to route any input to a given fixed output port. This is achieved by setting half of the phases to π and setting the other half to 0, or by applying 0 to all the phases to obtain a full swap. The $N \times N$ passive splitter can either be a $N \times N$ MMI or built from of 2×2 couplers. Fabricating large $N \times N$ balanced MMIs with low loss is challenging, so we propose using cascaded couplers (having a reflectivity of 0.5) and crossings as shown in Figs. 4b and 4c.

The lower bound on the probability to emit a triggered single photon q^*_{GMZ} is, from Eq. 15:

$$q^*_{GMZ} = p_{single}\eta_{delay}\left(1-(1-p_{trig})^N\right)\eta_{modulator}\eta^2_{N\times N}, \tag{20}$$

Source Type	Total number of phase modulators	Total number of directional couplers	Phase modulator depth	Coupler depth
Log Tree	$N-1$	$2(N-1)$	$\log_2(N)$	$2\log_2(N)$
GMZ	N	$\frac{N(N+\log_2(N)-1)}{4}$	1	$2(N-1)$

Table I: Comparison of the requirements and component depth between the log tree and generalized MZI architectures as a function of the number of HSPSs N. The first two columns give the total number of component of the given type required for building the switch. The last two columns provide the depth of the circuit for each component—or the number of components of each type that each photon has to go through.

where $\eta_{modulator}$ is the transmission of the modulator section and $\eta_{N\times N}$ is the loss induced by the balanced $N \times N$ switch. If implemented with couplers with transmission $\eta_{coupler}$, then $\eta_{N\times N} = \eta_{coupler}^{N-1}$. To show the effect of coupler loss, the optimal number of sources to achieve a probability of triggered single photon emission q^*_{GMZ} with $p_{single}\eta_{delay}\eta_{modulator} = 1$ is plotted in Fig. 5.

The choice between the log tree and the GMZ depends on the dominant component loss. In the GMZ, the photon must pass only a single phase modulator, instead of a logarithmic number as in the log-tree scheme. However, the GMZ requires a linear scaling in the number of directional couplers the photon passes through, instead of the logarithmic scaling given by the log tree scheme. Also, the GMZ requires $O(n^2)$ couplers while the total number of components for the log tree scales linearly. Table (1) shows a summary of the different resource scalings for the two architectures.

Since the switching network is balanced, the exact probability for emitting a triggered single-photon q_{GMZ} and the output state multi-photon contamination probability p^{GMZ}_{multi} are calculated as explained in section (II A) using $\eta_{network} = \eta_{delay}\eta_{modulator}\eta^2_{N\times N}$. We will consider these expressions further in section III.

D. Chained sources

In this scheme, unit cells—each composed of a HSPS, a delay line, and a 2×2 switch—are cascaded to build a chain of sources (Fig. 6a). The electrical output trigger of the HSPS directly drives a switch which routes the emitted photon to the output port while the input port is routed towards a blocked path. As in the other schemes, an optical delay line allows sufficient time for the detection of the idler photon and the configuration of the switch.

The chained scheme benefits from very simple control logic requirements, since each switch is only driven by one HSPS. For switches driven by voltage, for example, the logic consists only of amplifying the trigger signal from the HSPS to the required switching voltage. This switching logic privileges the HSPS emitting closest to the output of the chain, and hence the photon from the HSPS suffering the least from the losses. As an example, if two cells are cascaded and cell 2 triggers before cell 1, the switch corresponding to cell 1 will remove the photon from the HSPS of cell 2 and replace it with a new photon from the HSPS of cell 1.

Since the switching network applies different amounts of loss to the different HSPSs, we cannot derive the lower bound for the single-photon emission probability q^*_{chain} using the method given in Sec. II A. We therefore show a different derivation here. Given a chain of N unit cells, assuming HSPSs with a probability of triggering p_{trig}, a probability for the heralded state to be a single photon p_{single}, and switches with transmission η, q^*_{chain} is given by summing the probabilities for each source to fire given that the subsequent ones do not, and accounting for switching losses, which gives:

$$q^*_{chain} = p_{single}\eta_{delay}\sum_{n=1}^{N} p_{trig}\eta^n\left(1-p_{trig}\right)^{n-1}$$

$$= p_{single}\eta_{delay}p_{trig}\eta\frac{1-\left[\left(1-p_{trig}\right)\eta\right]^N}{1-\left(1-p_{trig}\right)\eta}. \tag{21}$$

The maximal probability for emitting a single photon is obtained in the limit of an infinite chain $q_{max} = p_{single}\eta_{delay}\frac{p_{trig}\eta}{1-(1-p_{trig})\eta}$. In practice, to operate at a fraction f of the maximal probability q^*_{max}, the length of the chain is given by solving $fq^*_{max} = p_{single}\eta_{delay}p_{trig}\eta\frac{1-[(1-p_{trig})\eta]^N}{1-(1-p_{trig})\eta}$ which gives:

$$N = \left\lceil \frac{\ln\left(1-x\right)}{\ln\left[\left(1-p_{trig}\right)\eta\right]} \right\rceil. \tag{22}$$

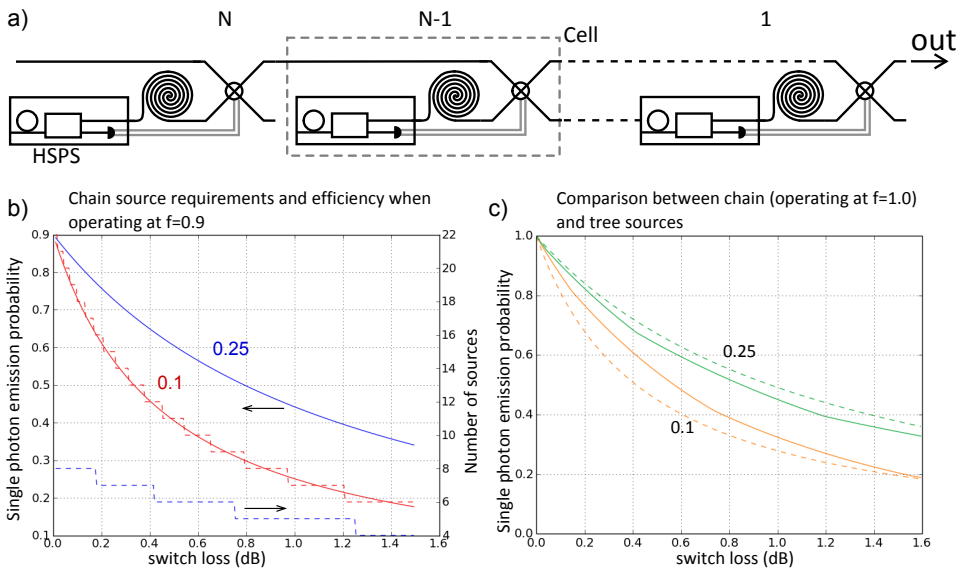

Figure 6: Chain MUX source and performance. a) Figure 6: Array of chained sources. N unit cells are cascaded to build a chained multiplexed single-photon source. A unit cell is composed of a HSPS, an optical delay line, and a 2 × 2 switch. b) Number of cells required (dash line, right axis) to achieve a maximal probability of triggered single-photon emission q^*_{chain} (plain line, left axis) as a function of the switch loss. We chose a fractional efficiency of f = 0.9 to compute the required number of cells. Two regimes are plotted corresponding to $p_{trig} = 0.1$ (red) and $p_{trig} = 0.25$ (blue). c) Comparison between the chained source (plain) and log tree (dashed) triggered single-photon emission probability, as a function of switch loss, for two different regimes, $p_{trig} = 0.1$ (orange) and $p_{trig} = 0.25$ (green). The optimal single-photon probability q^*_{max} is plotted for both the chain source—for f=1.0, corresponding to the limit of an infinite number of cascaded cells—and for the log-tree source—using the optimal number of switches.

We show the single-photon emission probability q^*_{chain} with $p_{single}\eta_{delay} = 1$ and the number of cells required N as a function of the switching loss for $f = 0.9$ in Fig. 6b. As with the log tree architecture, the required number of sources becomes impractical for small p_{trig}, but can be kept below 8 when operating at $p_{trig} = 0.25$. The performance of the chained scheme compares well with the performance of the log tree, as shown in 6c). It has better performances for $p_{trig} = 0.1$ (for a switch loss less than 1.6 dB) and is close to the log-tree performances for $p_{trig} = 0.25$.

The derivation for the exact probability of triggered single photon emission q_{chain} and the output state multi-photon contamination probability p^{chain}_{multi} are shown in Appendix B.

III. DISCUSSION: GENERATING M SINGLE PHOTONS USING M MULTIPLEXED SOURCES

Experiments with about 8 single photons represent the current state-of-the-art photon number for SPDC experiments in practice, so we will examine the performance of multiplexed sources for the generation of >10 single photons in separate spatial modes. We first consider using M log-tree multiplexed sources to generate M single photons at a rate of 100 Hz, assuming a pulsed laser seed with a repetition rate of 100 MHz, number-resolving detectors, and $p_{pair} = 0.1$. Fig. 7 shows the maximum tolerable switch loss for generating M single photons under these assumptions, and the resulting probability of multi-photon contamination in the output state for this same switch loss. We considered two values for the lumped idler detection efficiency (which includes filter loss), $\eta_i = 0.9$ and $\eta_i = 0.99$, and assumed that this loss is also applied to the signal channel. We see that with $\eta_i = 0.9$ and switches with 1 dB loss (~ 0.794 transmission), 14 single photons can be generated at the target 100 Hz rate with multi-photon contamination below 10% . Extending beyond this regime to perform experiments with 20-40 photons with less than 10% multi-photon contamination requires $\eta_i \approx 0.99$ lumped idler detection efficiency with 2x2 switches having each $< 0.4 - 0.2$ dB loss ($\sim 0.912 - 0.955$ transmission).

Although these numbers are beyond what is attainable using the current state-of-the-art components, they may be attainable in the near-to-mid-future with further development and integration. For reference, prototype all-optical switches in fiber have demonstrated insertion loss of ~ 0.6 dB (~ 0.871 transmission) [32], on-chip filters for sufficient pump suppression have demonstrated insertion loss of of ~ 0.8 dB (~ 0.832 transmission) [33], and state-of-the-art

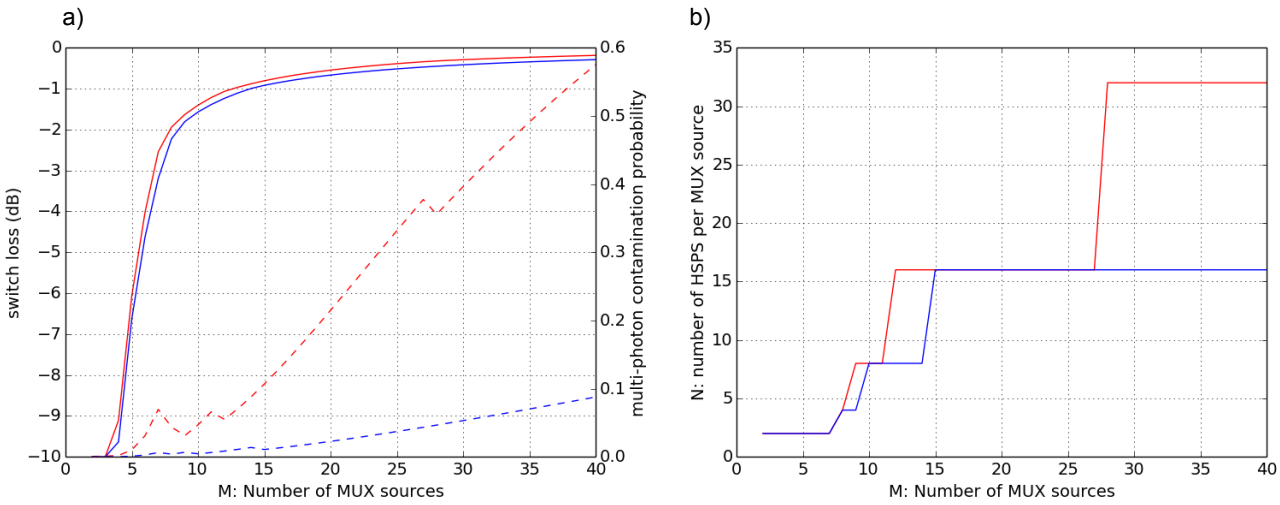

Figure 7: Left axis (plain lines):Requirements for generating M single photons at a rate of 100 Hz, from a 100 MHz pulsed laser for two different idler detection efficiencies. The red lines correspond to a lumped detection efficiency of $\eta_i = \eta_s = 0.9$. The blue lines correspond to a lumped detection efficiency of $\eta_i = \eta_s = 0.99$. a) Maximum tolerable switch loss (per 2x2 switch) vs number M of log-tree MUX sources operated in parallel. Right axis (dashed lines): probability of multi-photon contamination in output state from the M MUX sources when using the maximum tolerable switch loss. b) Number of HSPSs required per MUX source in order to meet the requirements in a).

single-photon detectors have demonstrated efficiencies of 0.93 [34]. Although the single-photon detectors referenced in [34] are non-number-resolving and are limited to a deadtime of 40 ns, we note that passive multiplexing techniques using arrays of detectors [35][36] can achieve approximate number-resolving capabilities and reduce deadtime. However, the exact effect of loss using these specific detector architectures on multiplexed sources, and their resource requirements, is beyond the scope of this paper.

For applications requiring a very large number of single-photons ($M \gg 40$), such as the universal quantum computer, error-correcting and loss-tolerant encodings can be used to achieve fault-tolerant computation, provided the error rates are below required thresholds. Meeting these thresholds will require sources with the highest single-photon emission probability and very low multi-photon contamination. We briefly consider what is attainable with optimistic long-term goals for the performance of required hardware components. Assuming 0.99 lumped idler detection efficiency, 2x2 switches with 0.98 transmission, and $p_{pair} = 0.1$, this corresponds to a multiplexed single-photon source efficiency of 0.8744, a multi-photon emission probability of 0.0017, and 64 HSPSs per MUX source. Using $p_{pair} = 0.25$, this increases the single-photon source efficiency to 0.8965 and reduces the resource requirements to 16 HSPS per MUX source, although at the cost of an increased multi-photon contamination probability of 0.0083. Further research is necessary to translate these single- and multi-photon emission probabilities into error rates for fault-tolerance in linear optical quantum computing, and to optimize multiplexed source architectures for scalable quantum computation.

IV. CONCLUSION

In our analysis we have studied multiplexed single-photon sources with photon loss and inefficient detectors. We derived expressions for single-photon emission probability and multi-photon contamination probability using number-resolving and non-number-resolving detectors for a general HSPS and for three MUX architectures: a log-tree switching scheme, a chained switching scheme, and a generalized MZI scheme.

Our findings indicate that number-resolving detectors offer a considerable advantage over threshold detectors for MUX sources, and are essential for MUX sources with the highest efficiency. The performance of the chained scheme compares well with the performance of the log tree, and has a simple logic requirements that may be beneficial for a near-term implementation. The GMZ offers an alternative switching structure that requires fewer phase modulators but more directional couplers than the other schemes.

All three of the architectures considered are capable of a high efficiency single-photon source with low multi-photon contamination if the components are close to ideal. For example, with a log-tree architecture composed of switches with $< 0.4-0.2$ dB loss ($\sim 0.912-0.955$ transmission) and number-resolving detectors with 99% efficiency, a single-photon source capable of producing a 100 Hz rate of 20-40 photon states with less than 10% multi-photon contamination is possible. Such a source would be a valuable resource for quantum technologies such as the boson sampling machine and quantum simulators. With lower-loss switches and the high efficiency detectors, a MUX source approaching the threshold requirements for a fully fault-tolerant universal quantum computer should be possible. Further work is necessary to find the optimal multiplexing schemes which could encompass the direct generation and multiplexing of multi-photon states or entangled resource states.

We thank Xiao-Qi Zhou, Joshua Silverstone, Jonathan Matthews, Anthony Laing, Daryl Beggs, and Jake Kennard for useful discussions and comments. This work was supported by Army Research Office (ARO) grant No. W911NF-14-1-0133.

Appendix A: Heralded single-photon source parameters derivation

Threshold detector

The source output state after accounting for losses is given by:

$$\hat{\rho} = \left(1-|\xi|^2\right)\left(\sum_{n=0}^{\infty}|\xi|^{2n}\sum_{p=0}^{n}\sum_{k=0}^{n}C_n^p\eta_i^p\left(1-\eta_i\right)^{n-p}C_n^k\eta_s^k\left(1-\eta_s\right)^{n-k}\hat{\rho}_{p,k}\right), \tag{23}$$

where $\hat{\rho}_{p,k} = |p\rangle_i |k\rangle_s \langle p|_i \langle k|_s$ and C_n^k is the binomial coefficient.

The probability for the detector placed on the idler arm to trigger is given by summing all the contribution of states having at least one photon. Starting with the reduced state after tracing out the signal mode:

$$p_{trig\,TD} = \sum_{m=1}^{\infty}\langle m|_i\left(1-|\xi|^2\right)\left(\sum_{n=0}^{\infty}|\xi|^{2n}\sum_{p=0}^{n}C_n^p\eta_i^p\left(1-\eta_i\right)^{n-p}|p\rangle_i\langle p|_i\right)|m\rangle_i$$

$$= \left(1-|\xi|^2\right)\left(\sum_{n=1}^{\infty}|\xi|^{2n}\sum_{p=1}^{n}C_n^p\eta_i^p\left(1-\eta_i\right)^{n-p}\right)$$

$$= \left(1-|\xi|^2\right)\left(\sum_{n=1}^{\infty}|\xi|^{2n}\left(\sum_{p=0}^{n}C_n^p\eta_i^p\left(1-\eta_i\right)^{n-p}-\left(1-\eta_i\right)^n\right)\right)$$

$$= \left(1-|\xi|^2\right)\left(\sum_{n=0}^{\infty}|\xi|^{2n}\left(1-\left(1-\eta_i\right)^n\right)\right)$$

$$= \left(1-|\xi|^2\right)\left(\frac{1}{1-|\xi|^2}-\frac{1}{1-|\xi|^2\left(1-\eta_i\right)}\right).$$

$$p_{trig\,TD} = \frac{|\xi|^2\eta_i}{1-|\xi|^2\left(1-\eta_i\right)}. \tag{24}$$

We can check the validity of the expression in the two extreme cases. If $\eta_i = 1$, the probability to trigger is maximal, $p_{trig} = |\xi|^2$. If $\eta_i = 0$ then $p_{trig} = 0$.

The heralded state in the signal arm is expressed, renormalizing by dividing by p_{trig}, as:

$$\hat{\rho}_{H\,TD} = \frac{\left(1-|\xi|^2\right)}{p_{trig\,TD}} \sum_{m=1}^{\infty} \langle m|_i \left(\sum_{n=0}^{\infty} |\xi|^{2n} \sum_{p=0}^{n} \sum_{k=0}^{n} C_n^p \eta_i^p \left(1-\eta_i\right)^{n-p} C_n^k \eta_s^k \left(1-\eta_s\right)^{n-k} \hat{\rho}_{p,k} \right) |m\rangle_i$$

$$= \frac{\left(1-|\xi|^2\right)}{p_{trig\,TD}} \left(\sum_{n=1}^{\infty} |\xi|^{2n} \sum_{p=1}^{n} \sum_{k=0}^{n} C_n^p \eta_i^p \left(1-\eta_i\right)^{n-p} C_n^k \eta_s^k \left(1-\eta_s\right)^{n-k} |k\rangle_s \langle k|_s \right).$$

We can compute the probability that the heralded state is a single photon using $p_{single\,TD} = \langle 1|_s \hat{\rho}_{heralded\,TD} |1\rangle_s$:

$$p_{single\,TD} = \frac{\left(1-|\xi|^2\right)}{p_{trig\,TD}} \left(\sum_{n=1}^{\infty} |\xi|^{2n} C_n^1 \eta_s \left(1-\eta_s\right)^{n-1} \sum_{p=1}^{n} C_n^p \eta_i^p \left(1-\eta_i\right)^{n-p} \right)$$

$$= \frac{\left(1-|\xi|^2\right)}{p_{trig\,TD}} \left(\sum_{n=1}^{\infty} |\xi|^{2n} C_n^1 \eta_s \left(1-\eta_s\right)^{n-1} \left(1-\left(1-\eta_i\right)^n\right) \right)$$

$$= \frac{\left(1-|\xi|^2\right)}{p_{trig\,TD}} |\xi|^2 \left(\eta_s \sum_{n=1}^{\infty} n |\xi|^{2(n-1)} \left(1-\eta_s\right)^{n-1} - \left(1-\eta_i\right) \eta_s \sum_{n=1}^{\infty} |\xi|^{2(n-1)} n \left(1-\eta_s\right)^{n-1} \left(1-\eta_i\right)^{n-1} \right).$$

Using the identity (obtained from taking the derivative of the geometric series) $\sum_{n=0}^{\infty} n x^{n-1} = 1/(1-x)^2$:

$$p_{single\,TD} = \frac{\left(1-|\xi|^2\right)}{p_{trig\,TD}} |\xi|^2 \eta_s \left(\frac{1}{\left(1-|\xi|^2\left(1-\eta_s\right)\right)^2} - \frac{\left(1-\eta_i\right)}{\left(1-|\xi|^2\left(1-\eta_s\right)\left(1-\eta_i\right)\right)^2} \right).$$

$$p_{single\,TD} = \left(1-|\xi|^2\right) \eta_s \frac{\left[1-\left(|\xi|^2\left(1-\eta_s\right)\right)^2\left(1-\eta_i\right)\right]\left[1-|\xi|^2\left(1-\eta_i\right)\right]}{\left[1-|\xi|^2\left(1-\eta_s\right)\right]^2\left[1-|\xi|^2\left(1-\eta_s\right)\left(1-\eta_i\right)\right]^2}. \tag{25}$$

In the lossless case, we obtain $p_{single\,TD} = \left(1-|\xi|^2\right)$, which, with a triggering probability $p_{trig} = |\xi|^2$ (from Eq. 24), is consistent with a probability of getting one photon of $|\xi|^2\left(1-|\xi|^2\right)$ (from Eq. 1).

The probability that the heralded state contains multi-photon contamination is derived as follows. First, we define:

$$Z_{TD} = \sum_{q=1}^{\infty} \sum_{m=1}^{\infty} \langle q, m| \hat{\rho} |q, m\rangle$$

$$= \left(1-|\xi|^2\right) \left(\sum_{n=1}^{\infty} |\xi|^{2n} \sum_{p=1}^{n} \sum_{k=1}^{n} C_n^p \eta_i^p \left(1-\eta_i\right)^{n-p} C_n^k \eta_s^k \left(1-\eta_s\right)^{n-k} \right)$$

$$= \left(1-|\xi|^2\right) \left(\sum_{n=1}^{\infty} |\xi|^{2n} \left(1-\left(1-\eta_i\right)^n\right) \left(1-\left(1-\eta_s\right)^n\right) \right)$$

$$= \left(1-|\xi|^2\right)\left(\sum_{n=1}^{\infty}|\xi|^{2n}\left(1+(1-\eta_s)^n(1-\eta_i)^n-(1-\eta_i)^n-(1-\eta_s)^n\right)\right)$$

$$= \left(1-|\xi|^2\right)|\xi|^2\left(\frac{1}{1-|\xi|^2}+\frac{(1-\eta_s)(1-\eta_i)}{1-|\xi|^2(1-\eta_s)(1-\eta_i)}-\frac{(1-\eta_i)}{1-|\xi|^2(1-\eta_i)}-\frac{(1-\eta_s)}{1-|\xi|^2(1-\eta_s)}\right).$$

Then it follows that $p_{multi\,TD}=\sum_{m=2}^{\infty}\langle m|_s\,\hat{\rho}_{heralded\,TD}\,|m\rangle_s$:

$$p_{multi\,TD}=\frac{Z_{TD}}{p_{trig\,TD}}-p_{single\,TD}. \tag{26}$$

Number-resolving detector

Now we consider the number-resolving detector. Starting with Eq. 2, tracing out the signal mode and calculating the probability to get only one photon:

$$p_{trig\,NRD}=\langle 1|_i\left(1-|\xi|^2\right)\left(\sum_{n=0}^{\infty}|\xi|^{2n}\sum_{p=0}^{n}C_n^p\eta_i^p(1-\eta_i)^{n-p}\,|p\rangle_i\langle p|_i\right)|1\rangle_i$$

$$= \left(1-|\xi|^2\right)\left(\sum_{n=1}^{\infty}|\xi|^{2n}C_n^1\eta_i(1-\eta_i)^{n-1}\right)$$

$$= \left(1-|\xi|^2\right)|\xi|^2\eta_i\left(\sum_{n=1}^{\infty}|\xi|^{2(n-1)}n(1-\eta_i)^{n-1}\right).$$

$$p_{trig\,NRD}=\frac{\left(1-|\xi|^2\right)|\xi|^2\eta_i}{\left(1-(1-\eta_i)|\xi|^2\right)^2}. \tag{27}$$

We can check the validity of the expression in the two extreme cases. If $\eta_i=1$, the probability to trigger is maximal, $p_{trig}=\left(1-|\xi|^2\right)|\xi|^2$. If η_i=0 then $p_{trig}=0$.

The corresponding heralded state is:

$$\hat{\rho}_{H\,NRD}=\frac{\left(1-|\xi|^2\right)}{p_{trig\,NRD}}\langle 1|_i\left(\sum_{n=0}^{\infty}|\xi|^{2n}\sum_{p=0}^{n}\sum_{k=0}^{n}C_n^p\eta_i^p(1-\eta_i)^{n-p}C_n^k\eta_s^k(1-\eta_s)^{n-k}\,\hat{\rho}_{p,k}\right)|1\rangle_i$$

$$= \frac{\left(1-|\xi|^2\right)}{p_{trig\,NRD}}\eta_i\left(\sum_{n=1}^{\infty}|\xi|^{2n}n(1-\eta_i)^{n-1}\sum_{k=0}^{n}C_n^k\eta_s^k(1-\eta_s)^{n-k}\,|k\rangle_s\langle k|_s\right).$$

As in the previous case, We can compute the probability that the heralded state is a single photon using $p_{single\,NRD}=\langle 1|_s\,\hat{\rho}_{heralded\,TD}\,|1\rangle_s$:

$$p_{single\,NRD}=\frac{\left(1-|\xi|^2\right)}{p_{trig\,NRD}}\eta_i\left(\sum_{n=1}^{\infty}|\xi|^{2n}n(1-\eta_i)^{n-1}n\eta_s^1(1-\eta_s)^{n-1}\right)$$

$$= \frac{\left(1-|\xi|^2\right)}{p_{trig\,NRD}} \eta_i \eta_s |\xi|^2 \left(\sum_{n=1}^{\infty} n^2 (1-\eta_i)^{n-1} (1-\eta_s)^{n-1} |\xi|^{2(n-1)} \right).$$

Using $\sum_{n=1}^{\infty} n^2 x^{n-1} = \sum_{n=1}^{\infty} n(n-1)x^{n-1} + \sum_{n=1}^{\infty} n x^{n-1} = \frac{2x}{(1-x)^3} + \frac{1}{(1-x)^2}$:

$$p_{single\,NRD} = \left(1-(1-\eta_i)|\xi|^2\right)^2 \eta_s \left(\frac{\left(1+(1-\eta_i)(1-\eta_s)|\xi|^2\right)}{\left(1-(1-\eta_i)(1-\eta_s)|\xi|^2\right)^3} \right).$$

The probability that the heralded state contains multi-photon contamination is derived as follows. First, we define:

$$Z_{NRD} = \sum_{m=1}^{\infty} \langle 1,m| \hat{\rho} |1,m\rangle$$

$$= \left(1-|\xi|^2\right) \left(\sum_{n=1}^{\infty} |\xi|^{2n} \sum_{k=1}^{n} C_n^1 \eta_i (1-\eta_i)^{n-1} C_n^k \eta_s^k (1-\eta_s)^{n-k} \right)$$

$$= \left(1-|\xi|^2\right) |\xi|^2 \left(\eta_i \sum_{n=1}^{\infty} |\xi|^{2(n-1)} n (1-\eta_i)^{n-1} \left(1-(1-\eta_s)^n\right) \right)$$

$$= \left(1-|\xi|^2\right) |\xi|^2 \eta_i \left[\frac{1}{\left(1-|\xi|^2(1-\eta_i)\right)^2} - \frac{(1-\eta_s)}{\left(1-|\xi|^2(1-\eta_i)(1-\eta_s)\right)^2} \right]$$

$$= \frac{\left(1-|\xi|^2\right)|\xi|^2 \eta_i \eta_s}{\left(1-|\xi|^2(1-\eta_i)\right)^2} \left(\frac{1-(1-\eta_s)\left(|\xi|^2(1-\eta_i)\right)^2}{\left(1-|\xi|^2(1-\eta_i)(1-\eta_s)\right)^2} \right).$$

Then it follows that the probability that the heralded state contains multi-photon contamination is given by $p_{multi\,NRD} = \sum_{m=2}^{\infty} \langle m|_s \hat{\rho}_{heralded\,NRD} |m\rangle_s$:

$$p_{multi\,NRD} = \frac{Z_{NRD}}{p_{trig\,NRD}} - p_{single\,NRD}. \tag{28}$$

$$p_{multi\,NRD} = \eta_s \frac{1-(1-\eta_s)\left(|\xi|^2(1-\eta_i)\right)^2}{\left(1-|\xi|^2(1-\eta_i)(1-\eta_s)\right)^2} - p_{single\,NRD}.$$

Appendix B: Chain source derivation

The exact probability of single-photon emission q_{chain} can be calculated as follows. The state from a chain of N sources is:

$$\hat{\rho}_D = \sum_{j=0}^{N-1} p_{trig\,D} \left(1 - p_{trig\,D}\right)^j \hat{\rho}_{j\,D},$$

where $\hat{\rho}_{j\,D}$ is the state heralded by an individual HSPS for which the signal arm goes through $j+1$ switches each having transmission η, and D is the type of detector (TD for threshold detector or NRD for number resolving detector).

For a number resolving detector:

$$\hat{\rho}_{j\,NRD} = \frac{\left(1 - |\xi|^2\right)}{p_{trig\,NRD}} \eta_i \left(\sum_{n=1}^{\infty} |\xi|^{2n} n \left(1 - \eta_i\right)^{n-1} \sum_{k=0}^{n} C_n^k \left(\eta_s^k \eta^{j+1}\right) \left(1 - \left(\eta_s \eta^{j+1}\right)\right)^{n-k} |k\rangle_s \langle k|_s \right).$$

For a threshold detector:

$$\hat{\rho}_{j\,TD} = \frac{\left(1 - |\xi|^2\right)}{p_{trig\,TD}} \left(\sum_{n=1}^{\infty} |\xi|^{2n} \sum_{p=1}^{n} \sum_{k=0}^{n} C_n^p \eta_i^p \left(1 - \eta_i\right)^{n-p} C_n^k \left(\eta_s \eta^{\mathbf{j}+1}\right)^k \left(1 - \left(\eta_s \eta^{\mathbf{j}+1}\right)\right)^{n-k} |k\rangle_s \langle k|_s \right).$$

The probability that the MUX source triggers is given by:

$$p_{trig}^{chain} = 1 - \left(1 - p_{trig}\right)^N.$$

The probability of single-photon emission conditioned on the MUX source triggering is given by:

$$\begin{aligned} p_{single\,D}^{chain} &= \frac{1}{p_{trig}^{chain}} \langle 1|_s \hat{\rho}_D |1\rangle_s \\ &= \frac{1}{p_{trig}^{chain}} \sum_{j=0}^{N-1} p_{trig\,D} \left(1 - p_{trig\,D}\right)^j p_{single\,j\,D}, \end{aligned}$$

where $p_{single\,j\,D}$ is the probability of single-photon emission for an individual HSPS heralding the state $\hat{\rho}_{j\,D}$ (calculated in the same way as in Section I but using $\hat{\rho}_{j\,D}$). Then we have:

$$q_{chain\,D} = p_{single\,D}^{chain} \times p_{trig\,D}^{chain}.$$

The probability of multi photon contamination conditioned on the MUX source triggering is given by:

$$p_{multi}^{chain} = \frac{1}{p_{trig}^{chain}} \sum_{j=0}^{N-1} p_{trig\,D} \left(1 - p_{trig\,D}\right)^j p_{multi\,j\,D}, \tag{29}$$

with

$$p_{multi\,j\,D} = \sum_{m=2}^{\infty} \langle m|_s \hat{\rho}_{j\,D} |m\rangle_s$$

$$= Z_{j\,D} - p_{single_j\,D},$$

where $Z_{j\,D}$ is the normalization constant for an individual HSPS heralding the state $\hat{\rho}_{j\,D}$ (calculated in the same way as in Sec. I but using $\hat{\rho}_{j\,D}$) Then we can rewrite 29 as:

$$p_{multi}^{chain} = \frac{Z_D^{chain}}{p_{trig}^{chain}} - p_{single\,D}^{chain},$$

where

$$Z_D^{chain} = \sum_{j=0}^{N-1} p_{trig\,D}\,(1 - p_{trig\,D})^j\,Z_{j\,D}.$$

[1] Nicolas Sangouard and Hugo Zbinden. What are single photons good for? *Journal of Modern Optics*, 59(17):1458–1464, 2012.

[2] Hugo Cable and Jonathan P. Dowling. Efficient generation of large number-path entanglement using only linear optics and feed-forward. *Phys. Rev. Lett.*, 99:163604, Oct 2007.

[3] Kishore T. Kapale, Leo D. Didomenico, Hwang Lee, Pieter Kok, and Jonathan P. Dowling. Quantum interferometric sensors. *Concepts of Physics II*, 2005.

[4] Alan Aspuru-Guzik and Philip Walther. Photonic quantum simulators. *Nat Phys*, 8(4):285–291, 04 2012.

[5] Keith R. Motes, Jonathan P. Dowling, and Peter P. Rohde. Spontaneous parametric down-conversion photon sources are scalable in the asymptotic limit for boson sampling. *Phys. Rev. A*, 88:063822, Dec 2013.

[6] E. Knill, R. Laflamme, and G. J. Milburn. A scheme for efficient quantum computation with linear optics. *Nature*, 409(6816):46–52, 01 2001.

[7] Peter W. Shor. Polynomial-time algorithms for prime factorization and discrete logarithms on a quantum computer. *SIAM J. Comput.*, 26(5):1484–1509, October 1997.

[8] Seth Lloyd. Universal quantum simulators. *Science*, 273(5278):1073–1078, 1996.

[9] Philippe Grangier, Barry Sanders, and Jelena Vuckovic. Focus on single photons on demand. *New Journal of Physics*, 6(1), January 2004.

[10] Michael Varnava, Daniel E. Browne, and Terry Rudolph. How good must single photon sources and detectors be for efficient linear optical quantum computation? *Phys. Rev. Lett.*, 100:060502, Feb 2008.

[11] M. D. Eisaman, J. Fan, A. Migdall, and S. V. Polyakov. Invited review article: Single-photon sources and detectors. *Review of Scientific Instruments*, 82(7):–, 2011.

[12] Marcelo D. Cunha Pereira, Francisco E. Becerra, Boris L. Glebov, Jingyun Fan, Sae W. Nam, and Alan Migdall. Demonstrating highly symmetric single-mode, single-photon heralding efficiency in spontaneous parametric downconversion. *Opt. Lett.*, 38(10):1609–1611, 2013.

[13] Andreas Christ and Christine Silberhorn. Limits on the deterministic creation of pure single-photon states using parametric down-conversion. *Physical Review A*, 85:023829+, February 2012.

[14] A. L. Migdall, D. Branning, and S. Castelletto. Tailoring single-photon and multiphoton probabilities of a single-photon on-demand source. *Physical Review A*, 66:053805+, November 2002.

[15] M. A. Broome, M. P. Almeida, A. Fedrizzi, and A. G. White. Reducing multi-photon rates in pulsed down-conversion by temporal multiplexing. *Opt. Express*, 19(23):22698–22708, November 2011.

[16] Boris L. Glebov, J. Fan, and A. Migdall. Deterministic generation of single photons via multiplexing repetitive parametric downconversions. *Applied Physics Letters*, 103(3):031115+, 2013.

[17] Evan Jeffrey, Nicholas A. Peters, and Paul G. Kwiat. Towards a periodic deterministic source of arbitrary single-photon states. *New Journal of Physics*, 6(1):100+, July 2004.

[18] Kevin T. McCusker and Paul G. Kwiat. Efficient Optical Quantum State Engineering. *Physical Review Letters*, 103:163602+, October 2009.

[19] T. B. Pittman, B. C. Jacobs, and J. D. Franson. Single photons on pseudodemand from stored parametric down-conversion. *Physical Review A*, 66:042303+, October 2002.

[20] Jeffrey H. Shapiro and Franco N. Wong. On-demand single-photon generation using a modular array of parametric downconverters with electro-optic polarization controls. *Opt. Lett.*, 32(18):2698–2700, September 2007.

[21] Luca Mazzarella, Francesco Ticozzi, Alexander V. Sergienko, Giuseppe Vallone, and Paolo Villoresi. Asymmetric architecture for heralded single-photon sources. *Phys. Rev. A*, 88:023848, Aug 2013.

[22] Jacob Mower and Dirk Englund. Efficient generation of single and entangled photons on a silicon photonic integrated chip. *Physical Review A*, 84:052326+, November 2011.

[23] ChristianTomás Schmiegelow and MiguelAntonio Larotonda. Multiplexing photons with a binary division strategy. *Applied Physics B*, 116(2):447–454, 2014.

[24] X. S. Ma, S. Zotter, J. Kofler, T. Jennewein, and A. Zeilinger. Experimental generation of single photons via active multiplexing. *Phys. Rev. A*, 83(4):043814+, April 2011.

[25] M. J. Collins, C. Xiong, I. H. Rey, T. D. Vo, J. He, S. Shahnia, C. Reardon, T. F. Krauss, M. J. Steel, A. S. Clark, and B. J. Eggleton. Integrated spatial multiplexing of heralded single-photon sources. *Nat Commun*, 4, 10 2013.

[26] Thomas Meany, Lutfi A. Ngah, Matthew J. Collins, Alex S. Clark, Robert J. Williams, Benjamin J. Eggleton, M. J. Steel, Michael J. Withford, Olivier Alibart, and Sébastien Tanzilli. Hybrid photonic circuit for multiplexed heralded single photons. *Laser and Photonics Reviews*, 8(3):L42–L46, 2014.

[27] A. J. F. Hayes, H. L. Haselgrove, Alexei Gilchrist, and T. C. Ralph. Fault tolerance in parity-state linear optical quantum computing. *Phys. Rev. A*, 82:022323, Aug 2010.

[28] W. P. Grice, A. B. U'Ren, and I. A. Walmsley. Eliminating frequency and space-time correlations in multiphoton states. *Physical Review A*, 64(6):063815+, November 2001.

[29] Christopher Gerry and Peter Knight. *Introductory Quantum Optics*. Cambridge University Press, November 2004.

[30] Peter P. Rohde and Timothy C. Ralph. Modelling photo-detectors in quantum optics. *Journal of Modern Optics*, 53(11):1589–1603, 2006.

[31] Peter P. Rohde and Timothy C. Ralph. Error models for mode mismatch in linear optics quantum computing. *Phys. Rev. A*, 73:062312, Jun 2006.

[32] Timothy M Rambo, Kevin McCusker, Yu-Ping Huang, and Prem Kumar. Low-loss all-optical quantum switching. In *Photonics Society Summer Topical Meeting Series, 2013 IEEE*, pages 179–180. IEEE, 2013.

[33] Seok-Hwan Jeong, Daisuke Shimura, Takasi Simoyama, Miyoshi Seki, Nobuyuki Yokoyama, Minoru Ohtsuka, Keiji Koshino, Tsuyoshi Horikawa, Yu Tanaka, and Ken Morito. Low-loss, flat-topped and spectrally uniform silicon-nanowire-based 5th-order crow fabricated by arf-immersion lithography process on a 300-mm soi wafer. *Opt. Express*, 21(25):30163–30174, Dec 2013.

[34] MarsiliF., VermaV. B., SternJ. A., HarringtonS., LitaA. E., GerritsT., VayshenkerI., BaekB., ShawM. D., MirinR. P., and NamS. W. Detecting single infrared photons with 93% system efficiency. *Nat Photon*, 7(3):210–214, 03 2013.

[35] H. Paul, P. Törmä, T. Kiss, and I. Jex. Photon chopping: New way to measure the quantum state of light. *Phys. Rev. Lett.*, 76:2464–2467, Apr 1996.

[36] D. Sahin, A. Gaggero, Z. Zhou, S. Jahanmirinejad, F. Mattioli, R. Leoni, J. Beetz, M. Lermer, M. Kamp, S. Höfling, and A. Fiore. Waveguide photon-number-resolving detectors for quantum photonic integrated circuits. *Applied Physics Letters*, 103(11):–, 2013.